A RAY TRACING BASED MODEL FOR 3D LADAR SYSTEMS

Tomas Chevalier

Division of Information systems, Swedish Defence Research Agency, FOI, Box 1165, 581 11 Linköping, Sweden

Keywords: 3D ladar, Laser radar, Sensor model, Ray tracing, BRDF, Atmosphere.

Abstract: This paper describes an approach to simulate long range laser based 3D imaging sensor systems. The model is based on a ray tracing principle where a large amount of rays are sent from a sensor towards the scene. The scene, the target surface, and the atmosphere affect the rays and the final light energy distribution is acquired by a receiver, where sensor data is generated. The approach includes advanced descriptions of the materials in the scene, and modeling of several effects in the atmosphere and the receiver electronics. A turbulence model is included to achieve realistic long range simulations. Examples of simulations and corresponding real world data collection are shown. Model validations are presented.

1 INTRODUCTION

During the last decade many sensors for 3D data registration has emerged on the commercial market. To determine optimal parameters for those sensors a number of sensor system models have been developed along with these systems. At FOI (the Swedish Defence Research Agency) the capability to model various 3D ladar systems has been developed. A 3D ladar (sometimes also called 3D laser radar) system illuminates the scene with a laser and by scanning or using a matrix detector it collects a 3D geometry description of the scene, usually together with the intensity response. Related works show some approaches and examples of modeling tools, but either some important parts are ignored, as the atmosphere simulations, or the models are too simplified.

The first step of simulation was focused on correctly retrieving the 3D geometry description, while further efforts advanced the model to consider many other aspects. Such aspects include the atmospheric scintillations, the variation in the reflectance of separate scene parts, the complete waveform generation, and the capability to model several different sensor system types for registering 3D data. The model described in this paper is developed for monostatic systems, where the transmitter and the receiver are placed on the same platform. This is a common design for 3D ladar systems. It is mainly implemented in Matlab, with some computationally heavy parts in Java and C++.

This paper describes the model developed at FOI and the physical-based framework that we use in our development. Section 2 describes the different available sensor system types that have been considered for modeling. Section 3 covers the model framework and theories, especially for the atmosphere propagation of the laser beam. Details on validation efforts are given in Section 4. Simulation examples follow in Section 5 and we conclude the paper in Section 6.

1.1 Related Work

At the beginning of the sensor simulation history some passive sensor models were effectively implemented into graphics software and even in hardware (Phong, 1975). The simulated sensors were virtual cameras, and the algorithms were based on fairly basic ray tracing methods.

These algorithms were developed into more physically correctness and to include more advanced sensors (Powell, 2000), who simulates FLIR sensors and ladar sensors using graphics software.

To make the simulations more realistic and physically correct, more customized surface reflections were required. Already in 1967 studies on the reflections from rough surfaces had been performed (Torrance, 1967), and partly based on this, a physical reflection model was developed in 1991 (He, 1991). Some implications of non-Lambertian reflections for machine vision was published in 1995 (Oren, 1995).

A large number of sensor modeling projects have been published during the years and during the last

decade a number of 3D laser sensor models have evolved. For instance the work behind a 3D imaging laser scanner model was published in 2005 (Ortiz, 2005) and in 2006 BAE systems published their work (Grasso, 2006) on a 3D imaging ladar sensor model.

An American initiative to develop a sensor simulation environment, called *Irma*, was started by the Munitions Directorate at AFRL in 1980. At the beginning the purpose was primarily passive IR (infrared) simulations, but now the program also includes radar and ladar simulation capabilities. A number of publications are showing this progress, for instance (Savage, 2006; Savage, 2007; Savage, 2008), where especially (Savage, 2006; Savage, 2007) covers the ladar sensor development.

In parallel, DSTL began the development of a simulation program, *CameoSim* (CAMouflage Electro-Optic SIMulation) (Moorhead, 2001), to primarily simulate passive electro-optical sensors. This simulation program is commercially available, but unfortunately, the ladar module (which was scheduled to be working a couple of years ago) seems to be postponed. Sources indicated further progress of their *burst illumination (BIL) simulation*, and in April 2008 they presented 3D imaging sensor simulation based on *CameoSim* (Harvey, 2008).

A similar approach to the methods presented in this report was performed by the *Center for Advanced Imaging Ladar* (CAIL), at the Utah State University. Their ladar seeker model, *LadarSim* (Budge, 2006), is also based on discrete ray tracing as the approach presented in this paper, but differs in some ways. As example they do not consider the atmosphere, which is a major issue for Ladar system performance, and their sub resolution pattern inside each laser pulse is a hexagonal grid instead of the common quadratic grid. *LadarSim* is not commercially available and therefore not possible to compare in detail to the model described in this paper.

There are also non-imaging simulation efforts (Espinola, 2007; Grönwall, 2007), where the aim is to assist in the sensor performance assessment, without the need of sensor images.

2 3D LADAR SYSTEMS

Laser based 3D imaging systems can be of many types, of which some are described in this section. The most basic *Time-of-Flight Laser Scanner* that sends out separate laser pulses and measure the time to the returning echoes, the *Burst Illumination Ladar* which camera controls the high-speed shutter syn-

chronized to the laser pulse to generate range slice images, and finally the *3D Flash Ladar*, which contain a range sensing matrix detector to acquire complete 3D data using only one single laser pulse.

2.1 Time-of-Flight Laser Scanner

The classic version of a 3D imaging laser system is the Time-of-Flight (TOF) laser scanner, which works as a range sensing single element detector mechanically scanned over the scene to collect a number of laser echoes, as in Figure 1. The direction and range of each measurement is acquired, and by using a common coordinate system for all echoes, the data is registered together. Advanced versions of this sensor system type allow the complete returning waveforms to be acquired.
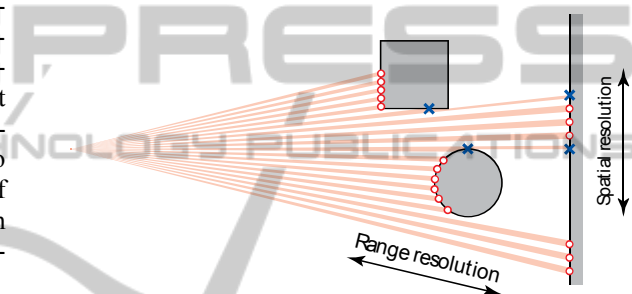
Figure 1: One-dimensional Time-of-Flight laser scanner illustration. The sensor system to the left edge is illuminating the scene to the right (each line is one pulse), where echoes are registered for each pulse, shown by circles and crosses. Crosses illustrate multiple echoes from one pulse.

2.2 Burst Illumination Ladar

The Burst Illumination Ladar, also called Gated Viewing system (Steinvall, 1999), consists of a short pulsed laser, a high-speed shutter, and a camera. This system uses an adjustable delay between the transmitted laser pulse and the high-speed shutter, while flooding the scene completely with a pulsed laser. The adjustable delay is used for temporal scanning, making it possible to register different range "slices" (or range gates) of the scene, which means to register light energy that is reflected towards the sensor from a certain distance, see Figure 2. Due to the possibility to use standard cameras, this sensor system type can have a very dense spatial resolution, high frame rate, or prf (pulse repetition frequency).

This sensor data needs post-processing to give range values in each pixel. This processing is based on stepping through a number of range slices and detecting peaks for each pixel. If interpolation is
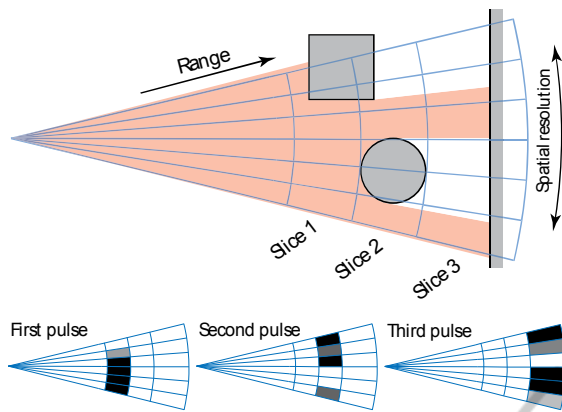
Figure 2: One-dimensional Burst Illumination Ladar system illustration. The left edge of the top image shows the sensor system flood illuminating the scene to the right, where the spatial resolution is set by the camera. The range dimension is binned by adjusting the delay between the emitted pulse and the shutter in the detector. One emitted pulse results in one registered slice, as shown in each of the bottom figures. The gray scale color in the rectangles illustrates the intensity in the echo, where white is high intensity, and black is low intensity.

performed the depth resolution can be a lot better than the distance between the slices (Andersson, 2006).

2.3 3D Flash Ladar

The 3D Flash Ladar system collects range data in a detector element matrix at a reasonable good frame rate. This makes it possible to register changes in a scene in three dimensions. Some systems only record range images while others record a complete waveform in each pixel, currently at the cost of low spatial resolution due to large sensor pixel elements. Figure 3 shows how this sensor system type records data.

This sensor system type is very interesting for future applications, especially since the data is formatted as range images and common straight-forward signal processing methods, like morphological operations, are applicable directly on the 3D data.

3 SENSOR DATA MODELING

All 3D ladar systems mentioned in Section 2 can be modelled using the same theory and framework although several parameters differ. This section describes the framework and main parts of the theory.
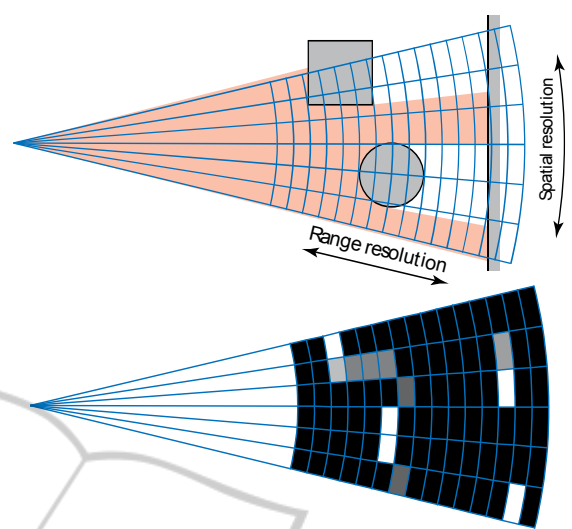
Figure 3: Two-dimensional 3D Flash Ladar system illustration. The scene to the right is flood illuminated from the left. The spatial resolution is set according to the detector matrix. The range dimension is binned inside the advanced detector elements, as shown in the bottom figure, where only one laser pulse is used to generate all the data. The gray scale color in the rectangles illustrates the intensity in the echo, where white is high intensity, and black is low intensity.

3.1 Model Framework

The model framework is built on four separated sections of settings; the *scene*, the *laser source*, the *atmosphere*, and the *receiver*.

° The *scene* settings define the geometry of all the objects in the scene, i.e. the physical environment that the sensor system will look at. It should also contain links to material descriptions, to allow advanced reflections according to measured material samples.

° The *laser source* settings define the way the scene is illuminated; both temporally and spatially.

° The *atmosphere* settings define the atmospheric conditions such as the turbulence strength and the aerial attenuation, see Section 3.4.

° The *receiver* settings define the receiver in the modelled system, together with its optics. The receiver spatial resolution sets the base resolution used throughout the simulation. This is multiplied by a sub resolution, determining the ability to image small details in the scene.

Each sub element is represented by a ray sent through the optics towards the scene. The propaga
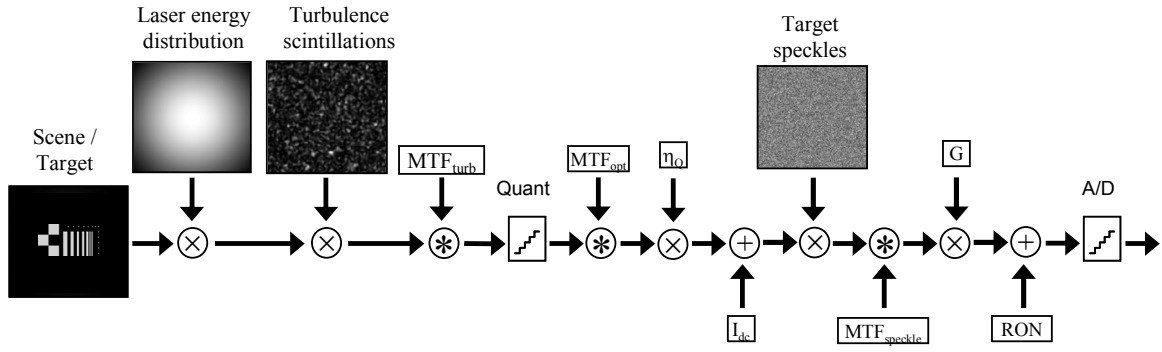
Figure 4: The model framework. One example scene (a reference board used for the validation measurements) is illuminated by a laser source, turbulence scintillations are multiplied and turbulence blurring effects are applied by convolution. The right of the 'Quant'-step contains the target speckle, the optics and the receiver effects. The contributions in this paper are mainly on the atmospheric simulations, and the quick but accurate combination with MTFs to simulate several types of signal disturbances.

tion of each ray is calculated in detail to detect intersections in the scene. Each of these intersections gives the information on which material is hit and in which angles the light incidents and reflects. Together with the laser spatial energy distribution, and the atmospheric scintillation, this information is used to determine the proportion of the transmitted light that finally hits the sensor element surface. The simulation framework is described in Figure 4, where the scene is illuminated by a laser source and affected by turbulence scintillations and blurring effects (MTF$_{turb}$). Further on, the signal energy is quantized into photons (Quant) and blurred even more by the receiver optics (MTF$_{opt}$). The receiver electronics defines the quantum efficiency (η_Q), the dark current noise (I_{dc}), the Gain (G), and the read-out-noise (RON). In the sensor we also see the target speckle effects together with blurring (MTF$_{speckle}$). Finally the signal is converted into a digitally recorded data by an A/D-conversion. In the figure, $\otimes$ means element-wise multiplication, $\circledast$ means convolution, and $\oplus$ means element-wise addition.

This figure only shows the spatial part of the energies, even though the temporal parts are well considered in all these model steps. The temporal parts are introduced by considering the scene as an impulse response to the three-dimensional energy distribution of the laser illumination.

The model parts containing the main contributions of this paper; the *material description*, the *atmosphere modeling*, and the *sensor data degradation*, are described in the following subsections, together with a fundamental system transfer function called the *laser radar equation*.

3.2 Laser Radar Equation

The one most fundamental relation these simulations are based upon is the laser radar equation (Jelalian, 1992), that describes the relation between the transmitted and the receiver energy as

$$P_r = P_T \cdot \eta_{syst} \cdot \left(\rho \cdot \frac{\pi r_a^2}{R^2} \right) \cdot e^{-2\sigma_{aer} R} \qquad (3\text{-}1)$$

It is derived from the well known radar equation (Skolnik, 2008), and identification of the three parts (to the right of P_T) in the equation tells us that the efficiency factor, η_{syst}, is the system efficiency. This is followed by the (parenthesized) BRDF, see Section 3.3, which consists of two factors; first the BRDF [sr^{-1}], ρ, and then the solid angle [sr] the receiver optics aperture covers as seen from the target reflecting the beam. The last factor, $e^{-2\sigma R}$, is the two-way aerial transmission due to aerosol particles in the atmosphere. The laser radar equation is used to attenuate each ray that passes through the atmosphere.

3.3 Material Reflections

To describe the surface reflection properties in detail the BRDF (bi-directional reflection density function), ρ, is used. The BRDF describes how an incident beam spreads into different angles. Figure 5 shows a BRDF example, where the amplitude is the portion of the energy that is reflected (per steradian) into a specific angle when a light source illuminates the surface from the direction parallel to the surface normal. The full BRDF descriptor allows a three-dimensional reflection distribution, but in our work we simplify it by using a two-dimensional approxi-

mation as in Figure 5, since we model a monostatic system. Also note that a specific BRDF is valid only for one wavelength.
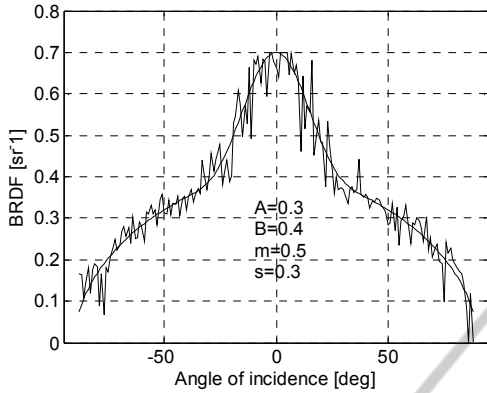

Figure 5: A synthetic BRDF example with the amplitude as a function of the reflected angle when the angle of incidence is parallel to the surface normal. Both a smooth and a noisy version are shown.

Even though BRDF measurements for several materials are available, we also need to model the BRDF analytically, to approximate the reflection properties for some materials. With some standard assumptions the BRDF definition (Steinvall, 1997) follows

$$\rho = \frac{Surface\ Radiance}{Surface\ Irradiance} = \frac{\dfrac{dP_s}{d\Omega_s}}{P_i \cos\theta_s} \approx \frac{\dfrac{P_s}{\Omega_s}}{P_i \cos\theta_s}, \qquad (3\text{-}2)$$

where the variables are depicted in Figure 6. The reflected solid angle is given by Ω_s. The incident and scattered light flux are represented by P_i and P_s. Finally, the angles of incidence and scattering are represented by θ_i and θ_s, respectively. In the monostatic system case, the angle of incidence coincides with the angle of the relevant scattering light, which gives us $\theta = \theta_s = \theta_i$.

There are advanced models to estimate the BRDF, which relate it to roughness, surface slope, correlation lengths, refractive index etc., but many of them tend to get unnecessary complicated. Some interesting simplified models have been published, and one of them, a one-dimensional version for monostatic systems, (Steinvall, 2000) is given by

$$\rho = \rho_{spec} + \rho_{diff} = \frac{A}{\cos^6(\theta)} e^{-\frac{\tan^2(\theta)}{s^2}} + B \cos^m(\theta) \qquad (3\text{-}3)$$

A and B are constants describing the relation between the specular and diffuse reflection. Specul reflection is the strong reflection where $\theta_s = \theta_i$ and
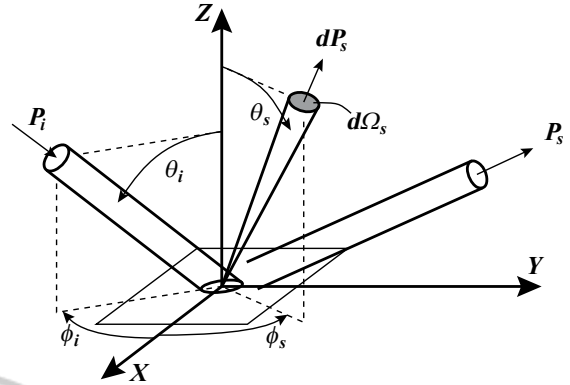
Figure 6: Description of the variables used in the BRDF definition. P shows the light flux while θ/ϕ are angles. The subscript s means *scattering/emitting* and i means *incident*. Ω_s is the solid angle. The figure is adapted from Steinvall (Steinvall, 2000).

$\phi_s = -\phi_i$. It can be recognized as the peak in the middle of Figure 5. The diffuse reflection supports the base reflection below the peak in the middle and covers reflection into almost any direction. The local slope is represented by s, and m is a parameter describing the diffuse surface. The angles of incidence and reflection are equal and represented by θ.

The BRDF is measured per steradian [sr^{-1}], which is defined as the solid angle of the reflected light. The following equation calculates the solid angle [sr] of the receiver aperture that is collecting the returning signal

$$\Omega_a = \frac{\pi r_a^2}{R^2} \qquad (3\text{-}4)$$

where r_a is the receiver aperture radius and R is the range to the target.

The practical use of the BRDF in the model includes a lookup table that connects the ray intersected surface, to a material in the database. If the material has measured BRDF data, that is used, otherwise a parameterized version is used to calculate the reflection according to equation (3-3).

3.4 Atmosphere Modeling

The turbulence in the atmosphere makes the propagating light deviate from the straight path, because of the variations in the aerial refractive index. This makes the signal of even a flat energy distribution from the transmitter to stochastically fluctuate at the range of the scene, as can be seen in Figure 7, where the square middle target is a unicolored reference board. The image show the target board, as seen

43

from the receiver close to the laser (two-way propagation).
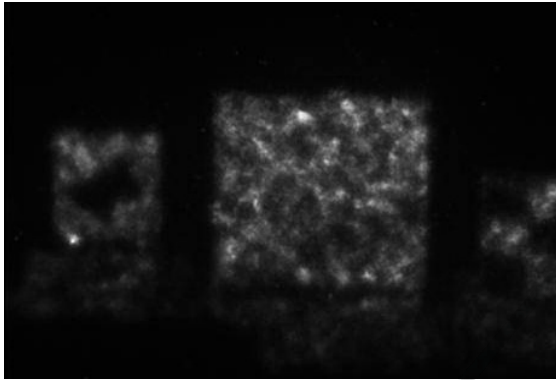
Figure 7: Two-way turbulence scintillations example at SWIR wavelength, with $C_n^2=1.15\cdot10^{-14}$. The image was acquired at 1km range with a FOI developed Burst Illumination Ladar system.

A very accurate way to simulate this behavior of the propagating beam is to use phase screens (Andrews, 1998; Andrews, 2001). However, simulations using phase screens are computationally very heavy. We have near real-time demands on our simulations and therefore we have chosen to use an approximation. In our simulation, the atmospheric effects are divided into the following approximately independent parts, where the theories are adapted from Andrews (Andrews, 1998; Andrews, 2001).

A. The beam Broadening, depends on turbulence strength (C_n^2) and the wavelength. It affects the spreading of the laser energy distribution that illuminates the scene.

B. The Turbulence Scintillations. The engineering approach used in the model is described in Section 3.4.1. The scintillation pattern is primarily based on a probability density function and a cell size equation, which describes the spatial pattern scale. The scintillations are multiplied to the laser energy as can be seen in Figure 4.

C. The Aerial Attenuation, which makes the pulse energy decrease as the range increases. This is due to smoke, fog, rain, and other particles in the air, and is a factor in the laser radar equation (3-1).

D. The Beam Wandering. The laser beam optical axis is randomly deflected by the turbulence in the air as it propagates through the atmosphere. This effect introduces a displacement of the energy returning from the scene.

E. The Distortion and Blurring effect, which can be seen in the images in Figure 7. A simplified way of modeling this is by using MTF (modulation transfer function) to blur the image. This corresponds to the MTF used in passive imagery, since it can be regarded as a one-way effect for the atmospheric propagation from the target into the receiver optics. The MTF is applied by convolution.

The turbulence strength (C_n^2) varies slowly over the day and reaches maximum at about noon, while the lowest values occur close to sunset and sunrise. This derives from the temperature gradient and wind velocity, which usually are lower at night, especially close to the shift between day and night. Close to the ground the turbulence is stronger than high up in the atmosphere.

3.4.1 Turbulence Scintillations

Statistically a distribution of intensities given as a pdf (probability density function) can be determined mathematically, according to equation (3-5). Even a turbulence cell size can be determined. Using these data a randomized turbulence scintillation pattern can be determined, as the example in Figure 8.
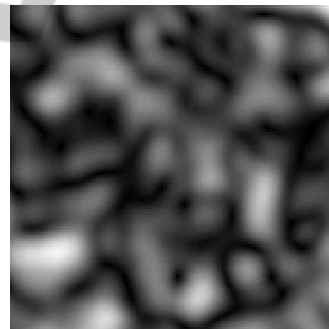

Figure 8: Simulated turbulence scintillation example according to equation (3-5).

The turbulence scintillation pdf during weak turbulence conditions is described (Andrews, 2001) by

$$P_{turb} = \frac{1}{S\cdot\sqrt{2\pi\sigma_{\ln I}^2}}\exp\left(-\left(\ln(\frac{S}{S_{av}})+\frac{1}{2}\sigma_{\ln I}^2\right)^2\Big/2\sigma_{\ln I}^2\right) \quad (3\text{-}5)$$

The pdf is based on the log-intensity variance, $\sigma_{\ln I}^2$, which depends on the target resolution as seen from the receiver, on the turbulence strength, and on the light wavelength.

The turbulence cell radius, ρ_l, is determined in relation to the spatial coherence radius of the current turbulence condition (Andrews, 2001) as in equation

44

(3-6), where R is the range, k is the wave number and ρ_0 is the spatial coherence radius. This turbulence cell radius is then used to spatially scale the simulated turbulence scintillation.

$$\rho_l = \frac{\sqrt{R/k}}{\sqrt{1 + R/\left(k\rho_0^2\right)}} \tag{3-6}$$

To generate the spatial intensity distribution, as the example in Figure 8, theory from Harris (Harris, 1995) is used as proposed by Letalick (Letalick, 2001). A randomized phase grid is generated, with rectangular distribution (which is used by Goodman (Goodman, 1984) in difference to Harris who uses Gaussian distribution). This random field is multiplied by a Gaussian function corresponding to a field distribution for the laser beam (TEM$_{00}$). The Fourier transform of the resulting matrix, the aperture function, gives the speckle field in the far field. By adjusting the spatial scale of the random noise and the diameter of the Gaussian field distribution, different scales and amplitudes for the speckle distribution can be achieved. In this way the speckle field can be matched to the probability density function in equation (3-5) and the turbulence cell size in (3-6).

3.5 Sensor Data Degradation

Several parts of the model cover sensor data degradation. The problem is not to simulate perfect undisturbed data, but to catch the most important degrading effects of the atmosphere, the scene and the sensor.

There already exist well described theories for sensor degradation of passive imaging, using MTF (modulation transfer function). This MTF is applied to passive imagery to decrease the effective resolution in a system, and can be separated into several parts, where the total system MTF is a multiplication of all separate MTFs; $MTF_{speckle}$ for the speckle limited resolution, MTF_{opt} for the diffraction limited (optical) resolution and MTF_{turb} for the turbulence limited resolution. The MTF are applied on the sensor data by convolution. As can be seen in Figure 9 the limiting MTF can be determined. The figure shows one-dimensional MTFs, even though the simulations are calculated in two dimensions, with radial symmetry.

The receiver unit contains the conversion from photons to a digital signal. This process introduces noise in many ways, for instance by the A/D-conversion quantization, the dark current background noise, and the read-out noise in the sensor

elements. This is modelled according to the model structure in Figure 4.
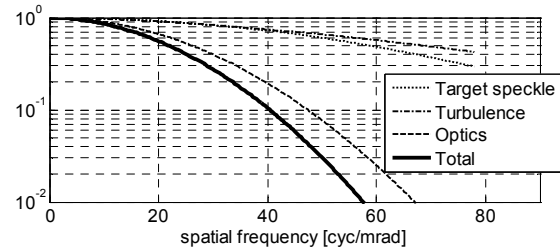
Figure 9: One system MTF example, where the optics is the limiting MTF and affects the total MTF the most.

4 SPATIAL DISTRIBUTION VALIDATION

This section describes the validation procedures and results for the spatial energy distribution. The model of the spatial energy distribution as a function of different turbulence levels is compared to outdoor measurements. First we validate the pdf of the energy distribution along with its cell size. Then we estimate the accuracy in the total system noise.

The first part is done using measurements at 1km range at weak and medium turbulence. The system (used for both measurements and simulations) is a burst illumination system at 532 nm. As can be seen in Figure 10, the visual resemblance is quite good between the measured (top row) and the simulated (bottom row) images. The correspondence between the energy distributions (histograms using all data in the images) is shown in the bottom row of the figure, where the solid line is the measured data, and the dashed blue line is the simulated data. The cell size is hard to measure exactly, but for this example the simulated cell size was about 16 pixels and the measured cell size was about 14 pixels, which we consider to be within reasonable interval.

The same data collection was used for the second part of the validation. Figure 11 show the chosen profile that was compared for a set of data and corresponding simulations. The white line in the top figure is chosen as the validation profile and it was compared between the measured and the simulated data as can be seen in the lower figure. The bias and the gain was compared in the complete data set and showed to fit quite well.
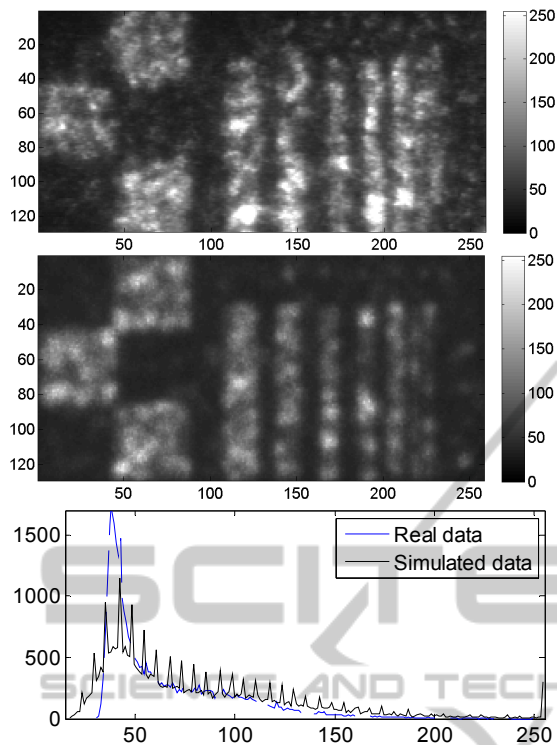
Figure 10: Validation of spatial energy distribution, where the top row is measured data on a reference board and the middle row is the simulated corresponding data. The bottom row shows a comparison between the energy distributions (histograms of all image data in the top images), where the measured data is shown with solid black line and simulated with dashed blue line.
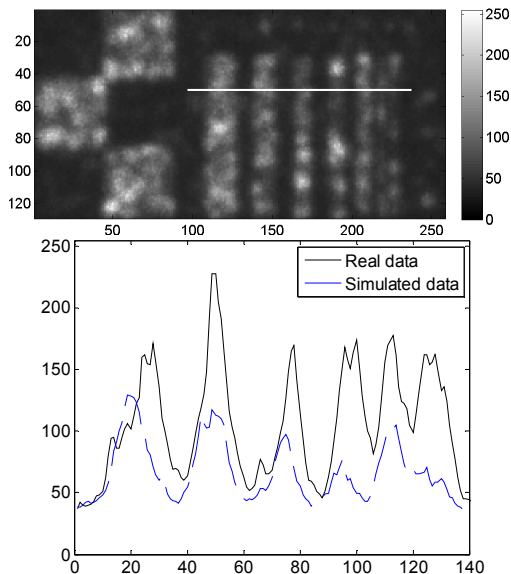

Figure 11: One validation example, where the profile marked with the white line in the top simulated image is shown in the bottom. The true measured profile is shown as the dashed line.

5 EXAMPLES

The flexible capabilities of the model are shown with some examples; B*urst Illumination Ladar*, *3D Flash Ladar,* and *Range Profiling Ladar*.

5.1 Burst Illumination Ladar

Parameters for a Burst Illumination Ladar were set up to validate the spatially high resolved turbulence effects. The example in Figure 10 shows measured data as well as simulated data from a Burst Illumination Ladar system with the target being a reference resolution board at 1 km range.

5.2 3D Flash Ladar

The currently most advanced 3D imaging sensor system, the 3D Flash Ladar, was modelled including the range detection in each pixel, which resulted in a set of points (128×128) from each frame. The simulations included a sensor movement during data capture, and the registered data can be seen in Figure 12.
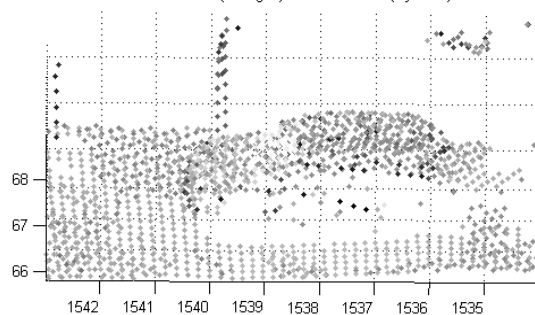

Figure 12: Simulated 3D Flash Ladar example. The target vehicle on top row is measured from a number of angles, in the environment seen in the middle row, and the data is globally registered in a common coordinate system, as shown on bottom row.

The top row shows the target vehicle which was placed on ground in a forested scene as seen on the middle row. The bottom row shows the globally registered points from five frames, collected from separate viewing directions.

5.3 Range Profiling Ladar

The capability to simulate waveforms is illustrated by this one dimensional simulation, where an aircraft, JAS 39 Gripen, is flood illuminated with a single laser beam, and all returning energy is collected into one single waveform. The top row in Figure 13 shows the target air craft that is illuminated from the left and the bottom row shows the returning echo.
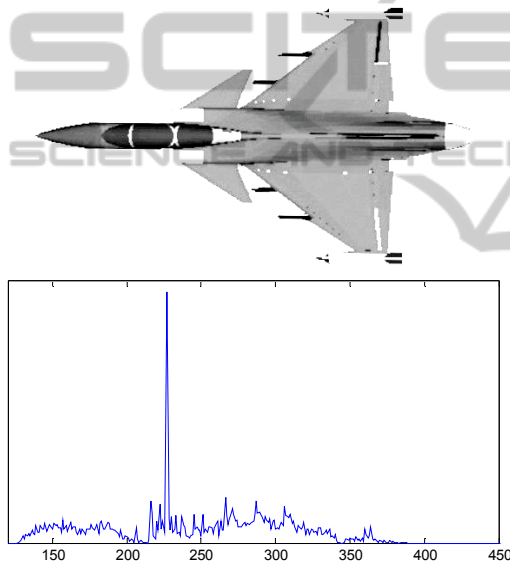
Figure 13: Range profiling simulation of the JAS 39 Gripen. The top row shows the target that is flood illuminated with a laser from the left, and the returning echo waveform is shown below. Note the peak which corresponds to the engine covers that were present at the aircraft model.

6 CONCLUSIONS

We have developed a model to simulate complex 3D ladar systems. It is a model that combines imaging of advanced scenario setups with atmospheric turbulence modeling as well as allowing degrading sensor effects to affect the resulting data. The simulation framework is divided into four fundamental parts; the scene, the laser source, the atmosphere and the receiver.

Earlier models developed for ladar simulations mostly lack the capability to simulate the atmos-

phere, or is not flexible enough to simulate several types of systems. A key contribution with this paper is therefore the atmospheric turbulence modeling that fits a fairly simple scintillation pattern to the advanced theory for laser beam propagation. We have also presented that this turbulence modeling can be applied to a complete system model that is flexible and capable of modeling a number of sensor system types. Finally, we have shown that the use of advanced material reflections (BRDF) can be applied upon the commonly used ray tracing methods.

We have successfully validated some parts of the model but also identified difficulties to validate the atmospheric simulations due to some stochastically varying entities. One important issue causing this problem is the lack of measurement data, since some atmospheric parameters uncontrollably varies during acquisition. Another important issue is that the knowledge about the parameters inside many of the sensor systems are proprietary information and therefore confidential.

REFERENCES

Andersson, P., 2006. Long range 3D imaging using range gated laser radar images. *Optical Engineering,* 45.

Andrews, L. C. & Phillips, R. L., 1998. *Laser Beam Propagation through Random Media,* Bellingham, Washington, USA, SPIE Press.

Andrews, L. C., Phillips, R. L. & Hopen, C. Y., 2001. *Laser Beam Scinitillation with Applications,* Bellingham, Washinton, USA, SPIE Press.

Budge, S., Leishman, B. & Pack, R., 2006. Simulation and modeling of return waveforms from a ladar beam footprint in USU LadarSIM. *SPIE Defence & Security, Laser Radar Technology and Applications XI,* Orlando, FL, USA, 62140N.

Espinola, R. L., Teaney, B., Nguyen, Q., Jacobs, E. L., Halford, C. E. & Tofsted, D. H., 2007. Active imaging system performance model for target acquisition. *SPIE Defense & Security Symposium, Infrared Imaging Systems: Design, Analysis, Modeling, and Testing XVIII,* Orlando, FL, USA, 65430T.

Goodman, J. W., 1984. Statistical Properties of Laser Speckle Patterns. IN DAINTY, J. C. (Ed.) *Topics in Applied Physics: Laser Speckle and Related Phenomena.* 2nd ed., Springer-Verlag.

Grasso, R. J., Dippel, G. F. & Russo, L. E., 2006. A model and simulation to predict 3D imaging LADAR sensor systems performance in real-world type environments. *SPIE Atmospheric Optical Modeling, Measurement, and Simulation II,,* 63030H.

Grönwall, C., Steinvall, O., Gustafsson, F. & Chevalier, T., 2007. Influence of laser radar sensor parameters on range-measurement and shape-fitting uncertainties. *Optical Engineering,* 46**,** 106201.

Harris, M., 1995. Light-field fluctuations in space and time *Contemporary Physics,* 36**,** 215-233.

Harvey, C., Wood, J., Randall, P., Watson, G. & Smith, G., 2008. Simulation of a new 3D imaging sensor for identifying difficult military targets. *SPIE Defense & Security Symposium, Laser Radar Technology and Applications XIII***,** Orlando, FL, USA, 69500I.

He, X. E., Torrance, K. E., Sillion, F. X. & Greenberg, D. P., 1991. A Comprehensive Physical Model for Light Reflection. *18th annual conference on Computer graphics and interactive techniques*, 175-186.

Jelalian, A. V., 1992. *Laser Radar System,* Norwood, MA, Artech House.

Letalick, D., Carlsson (later Grönwall), C. & Karlsson, C., 2001. A speckle model for laser vibrometry. *11th Coherent laser radar conference***,** Great Malvern, UK, 44-47.

Moorhead, I. R., Gilmore, M. A., Houlbrook, A. W., Oxford, D. E., Filbee, D. R., Stroud, C. A., Hutchings, G. & Kirk, A., 2001. CAMEO-SIM: a physics-based broadband scene simulation tool for assessment of camouflage, concealment, and deception methodologies. *Optical Engineering* 40**,** 1896-1905.

Oren, M. & Nayar, S. K., 1995. Generalization of the Lambertian model and implications for machine vision. *International Journal of Computer Vision* 14**,** 227-251.

Ortiz, S., Diaz-Caro, J. & Pareja, R., 2005. Radiometric Modeling of a 3D Imaging Laser Scanner. *SPIE Electro-Optical and Infrared Systems: Technology and Applications II*, 598709.

Phong, B. T., 1975. Illumination for Computer generated pictures. *Communications of the ACM,* 18**,** 311-317.

Powell, G., Martin, R., Marshall, D. & Markham, K., 2000. Simulation of FLIR and LADAR data using graphics animation software. *The Eighth Pacific Conference on Computer Graphics and Applications***,** Hong Kong, 126-134.

Savage, J., Coker, C., Edwards, D., Thai, B., Aboutalib, O., Chow, A., Yamaoka, N. & Kim, C., 2006. Irma 5.1 multi-sensor signature prediction model. *SPIE Defense & Security Symposium, Targets & Backgrounds XII: Characterization and Representation***,** Orlando, FL, USA, 6239OC.

Savage, J., Coker, C., Thai, B., Aboutalib, O., Chow, A., Yamaoka, N. & Kim, C., 2007. Irma 5.2 multi-sensor signature prediction model *SPIE Defense & Security Symposium, Modeling and Simulation for Military Operations II***,** Orlando, FL, USA, 656403.

Savage, J., Coker, C., Thai, B., Aboutalib, O. & Pau, J., 2008. Irma 5.2 multi-sensor signature prediction model *SPIE Defense & Security Symposium, Modeling and Simulation for Military Operations III***,** Orlando, FL, USA, 69650A.

Skolnik, M. I., 2008. *Radar Handbook,* New York, USA, McGraw-Hill.

Steinvall, O., 1997. Theory for laser systems performance modelling. Linköping, FOA. FOA-R--97-00599-612--SE.

Steinvall, O., Olsson, H., Bolander, G., Carlsson (later Grönwall), C. & Letalick, D., 1999. Gated Viewing for target detection and target recognition. *SPIE Laser Radar Technology and Applications IV***,** Orlando, FL, USA, 432-448.

Steinvall, O., 2000. Effects of target shape and reflection on laser radar cross sections. *Applied Optics,* 39**,** 4381-4391.

Torrance, K. E. & Sparrow, E. M., 1967. Theory for off-specular reflection from roughened surfaces. *Journal of the Optical Society of America,* 57**,** 1105-1114.